Proceedings of ASME Turbo Expo 2025
Turbomachinery Technical Conference and Exposition
GT2025
June 16-20, 2025, Memphis, Tennessee

GT2025-153216

MULTIPHYSICS OPTIMIZATION OF AN ELECTRO-DYNAMIC FILTER FOR GAS TURBINE

Mattia Piovan[1,*], Michele Pinelli[1], Alessio Suman[1], Nicola Zanini[1], Stefano Rossin[2], Stefano Minotti[2]

[1]University of Ferrara, Via Saragat 1, Ferrara (IT), 44122
[2]Baker Hughes Srl, Via Felice Matteucci 2, Firenze (IT) 50127

ABSTRACT

Fouling, corrosion, and erosion are the significant particle ingestion degradation phenomena that can occur in a gas turbine. The solid contaminants carried by the airflow enter the gas turbine, and depending on their chemical properties and particle size, they can adhere to the internal surfaces (fouling), remove some material (erosion), or react with the internal part (corrosion). For this reason, multi-stage filtration systems are commonly employed to preserve the life and the efficiency of the entire system. Mechanical filters are used to separate small-diameter particles by trapping the contaminant in cartridges of porous material. These devices are characterized by high filtration efficiency, but also high pressure drop, which increases with the exposure time. Inertial filters are used to separate large-diameter particles. However, due to their lower collection efficiency and pressure drop than porous filters, they are usually used in the pre-filtration stages. In recent years, electrostatic fields induced on dust-laden flows proved effective in trapping conductive particles and showing good potential for industrial applications.

This work shows a geometrical multi-physics optimization of a combined electrostatic-inertial filtration system. The combination of an electrostatic filter with an inertial one aims to take advantage of both the filtration mechanisms, i.e., capture efficiency comparable to a high-filtration system and a pressure drop comparable to an inertial one. A numerical campaign of the innovative type of filter is performed using an in-house OpenFOAM lagrangian solver that can simulate dispersed flows in the presence of an electrostatic field. Regarding geometrical optimization, a simplicial homology optimizer is used to find the geometry characterized by the highest capture efficiency and the lowest possible pressure drop.

Keywords: OpenFOAM, electrostatic solver, multi-physics optimization, gas turbine, filtration system, particle separation

*Corresponding author: mattia.piovan@unife.it

NOMENCLATURE

D_i	Ion diffusion coefficient
DC	Direct Current
E	Electric field
E_p	Electric field using the Peek condition
EPA	Efficiency Particulate Air filter
ESP	Electro Static Precipitator
FOD	Foreign Object Damage
F_{el}	Electrostatic Force
GT	Gas Turbine
HEPA	High Efficiency Particulate Air filter
J	Electric current
K	Ionic mobility in air
Q_p	Particle electric charge
r_c	Cylindrical electrode radius
SHGO	Simplicial Homology Global Optimizer
U_g	Gas velocity
V	Electric potential field
μ	Gas dynamic viscosity
μ_{eff}	Effective viscosity = $\mu + \mu_T$
μ_T	Turbulence viscosity
η_c	Capture efficiency
ρ_c	Ionic charge density
ρ_g	Gas density
ϵ_0	Dielectric permittivity of free space
ϵ_r	Particles relative magnetic permittivity
d_p	Particle diameter

1. INTRODUCTION

The gas turbine's filter house is the fundamental component used to preserve the life and efficiency of the entire system [1, 2]. The filters are used to avoid ingesting foreign objects that could damage (FOD) the compressor blades or partially block the passage area, causing an alteration of the fluid dynamics inside the machine. Moreover, the filtering media reduces the total amount of environmental contaminants ingested by the system. The pollutant particles that enter a gas turbine are responsible for

three main phenomena: fouling, erosion, and corrosion. These mechanisms affect the shape of the blade and cause performance degradation over time [3, 4]. The operating temperature, particle size, and the interaction between the blades and particles materials determine which mechanism prevails over the others. Fouling usually affects the compressor, and it is caused by the adherence of micro-sized particles [5, 6] on both stationary and rotating vanes. The turbine, instead, is mostly affected by erosion due to the impact between the ingested contaminants and the internal surfaces of the machine [7].

The efficiency of a filtration system depends on the particle size and airflow velocity. For this reason, a combination of filtration mechanisms is usually employed to have high filtration efficiency for a wide range of particle diameters [8]. The most used separation mechanisms for gas turbine applications are inertial, mechanical, and electrostatic. Inertial filters are employed as the first filtration stage to separate droplets and big particles (> 1 μm) from the air stream. The principle is related to the lower reactivity of particles with a high Stokes number to follow the flow. The filtration efficiency of inertial filters varies with the dimensions of the contaminants. In particular, they exhibit high efficiency for contaminants with large dimensions and low efficiency for small-sized contaminants. For this reason, mechanical filters are positioned downstream of the inertial one to collect a wide range of particle diameters at the intake of a gas turbine. Mechanical filters utilize fiber material to remove contaminants from the air stream. According to the European Standard EN1822-1 [9], mechanical filters can be divided into distinct categories based on their respective capture efficiency concerning a predetermined particle size. The most common filters are those designated as HEPA and EPA, which can achieve a filtration efficiency of up to 99.995 % by removing particles that are extremely small, with a size greater than 0.3 μm. The main disadvantage of these filters is the significantly higher pressure drop than an inertial filter. Furthermore, throughout its operational lifetime, an inertial filter is distinguished by a constant pressure loss, whereas a mechanical filter is characterized by an increase in pressure loss, which is attributed to the flow obstruction caused by the trapped particles. The fiber of a mechanical filter could be pre-charged before the installation to increase the capture efficiency, these filters are usually called electrostatic porous medium [8]. The advantage is related to the higher capture efficiency with extremely small particles, thanks to the action of the electrostatic force. The disadvantage of these devices is mainly associated with the decrease in time of performance due to the fading of the electrostatic force. In fact, after a certain amount of time, they act as a traditional porous medium, thereby losing the effects associated with the presence of electric charge.

Electrostatic precipitators, ESP, are another filtration system that uses electrostatic force to separate micro-sized particles, < 0.1 μm. These types of filters are not commonly used in the gas turbine sector. However, preliminary studies have been conducted [10] showing a very high potential for implementation in these applications. The particle separation occurs utilizing the corona effects, therefore using a strong electric field, which ionizes the air and charges the particles but does not create a voltaic arc within the filter. The generated electric field induces an electrostatic force on the particles, which pushes them onto a ground-collecting surface.

In previous works [11, 12], the effectiveness of an electrostatic inertial filter for gas turbine application has been proved numerically and experimentally. To simulate an electrodynamic filter and solve simultaneously the electric field and the flow field, the authors have developed a new lagrangian solver in the OpenFOAM environment [11]. The solver has been validated against two simplified literature test cases [13–15] for both continuous and discrete phases. The effects of different parameters, i.e., number of electrodes, geometry, and applied potentials, have been evaluated using the in-house solver. The final configuration is characterized by a powerful electric potential of 45 kV on the electrode surfaces. With this filter element, a numerical capture efficiency of approximately equal to 99 % has been obtained with a very low-pressure drop equal to 50 Pa.

The present study aims to optimize the filter element shape for a lower power supply system, which exhibits a maximum electric potential of 12 kV. The shape optimization is performed with the object to restore the performance losses due to the lower electric potential applied. For this reason, a multiphysics optimizer is developed in Python programming languages. Firstly, different types of geometrical parametrization of the filter are proposed. Subsequently, a Simplicial Homology Global Optimized (SHGO) is used to find the best solution for capture efficiency and pressure losses. The optimization process is conducted using a computational fluid dynamics (CFD) approach, specifically, the in-house Lagrangian solver developed in [11], is employed to calculate the capture efficiency and the pressure drop of the filter for each geometry. Different geometrical constraints have been added to avoid the presence of breakdown phenomena and to realize the filter element modularly. Furthermore, a threshold value for maximum acceptable pressure losses is established to ensure the system does not exceed the values typically associated with traditional filtration systems commonly employed in gas turbines.

2. METHODOLOGY

In the first part of the section, a brief description of the electrostatic lagrangian solver used to evaluate the performance of the electro-dynamic filter is reported. Subsequently, two types of geometrical parameterizations for the filtering elements are proposed. Finally, the optimization tool used to identify the geometry that provides the optimal balance between pressure losses and capture efficiency is presented.

2.1 Electrostatic solver description and CFD setup

In an electro-dynamic filter, both particles and fluid are subject to the influence of a strong electric field. The simultaneous resolution of the electric and fluid-dynamics fields is not a capability typically available within the usual commercial CFD software. For this reason, the OpenFOAM software is selected for this particular application. The open-source nature of the code permits the incorporation of novel solvers and supplementary features. In a previous study, the authors developed a new Lagrangian electrostatic solver, named *denseElectricParticleFoam*. The continuous phase was validated against the experimental literature data of Penny and Matick [13] evaluating the electric po-

tential trend inside the fluid domain. The discrete phase, instead, was validated against both numerical [15, 16] and experimental [14] literature data evaluating the particles' transverse velocity along the flow direction. A comprehensive overview of the implementation and the validation process are reported in [11]. The subsequent discussion briefly addresses the equations used inside the solver.

The conservation equations must be modified to take into account the presence of a strong electric field which affects not only the particles' behavior but also the continuous medium. In particular, the conservation of the momentum must be modified by adding a source term related to the Coulomb force exerted on the gas molecules. The momentum equation used in the *denseElectricParticleFoam* solver is (1), where ρ_c is the ionic charge density and $\mathbf{E}$ is the electric field. Other equations are necessary to solve simultaneously the electrostatic field and the flow, which are the Gauss's law (2), the irrotationality of the electric field (3), and the transport equation for the ionic density (4). In accordance with the literature, in the transport equation for the ionic density, the ionic mobility, K, and the ionic diffusivity are set respectively equal to 0.22 x 10^{-3} m^2 C/J and 0.2 m^2/s.

$$\rho_g \left[\frac{d\mathbf{U}_g}{dt} + \nabla \cdot \mathbf{U}_g \otimes \mathbf{U}_g \right] = -\nabla p + \mu_{eff} \nabla^2 \mathbf{U}_g + \rho_c \mathbf{E} \tag{1}$$

$$\nabla \cdot \mathbf{E} = \frac{\rho_c}{\varepsilon_0} \tag{2}$$

$$\mathbf{E} = -\nabla V \tag{3}$$

$$\mathbf{J} = \rho_c (K\mathbf{E} + \mathbf{U}_g) - D_i \nabla \rho_c \tag{4}$$

When conductive particles flow within an electrostatic field, they become electrically charged. The charging process is divided into diffusion charging and field charging [17]. The prevalence of one mechanism over the other depends on the particle charge compared to the saturation value. In particular, when the particle charge is lower than the saturation value, the most important mechanism is the field charging. Conversely, the diffusion charging prevails to the field one. The model proposed by Lawless [18] is used to model the charging process within the solver. Subsequently, the lagrangian force balance is modified to introduce the electrostatic force defined according to (5). The equations on the basis of the Lawless model, which are used to calculate the particle charge, Q_p, are reported in [11].

$$F_{el} = Q_p \mathbf{E} \tag{5}$$

In an ESP, the electric current flows between the electrodes and the grounded surfaces without creating a voltaic arc. This phenomenon is usually known as corona effect. The electric field on the electrode must satisfy Peek's condition (6). This condition establishes that the mean value of the electrostatic field module on the electrodes depends only on the geometrical properties and not on the applied potential. Therefore, a new boundary condition, Peek, is defined to calculate the ionic charge density on the boundary so that the gradient of E is consistent with Peek's condition. However, the condition reported in (6) is valid only for cylindrical electrodes. In the case of other shapes, the experimental voltage-current relationship must be implemented to find the ion density.

$$|\mathbf{E}_p| = 3.1 \text{ x } 10^6 \left(1 + \frac{0.308}{\sqrt{r_c}}\right) \tag{6}$$

The numerical domain used to simulate the electro-dynamic filter is reported in Fig.1. To reduce the computational effort of the simulation, only a 2D portion of the filter is simulated. For this reason, a symmetric boundary condition is applied to the upper and the lower surfaces. Moreover, at the inlet of the domain, an airflow velocity equal to 1 m/s is imposed, while at the outlet, a relative static pressure equal to 0 Pa is prescribed. Regarding the boundary condition relative to the presence of the electric field on the electrodes, indicated with red dots in Fig.1, a constant DC potential and the Peek condition for the ρ_c-E characteristic are applied. The filter element surfaces are divided into insulated and grounded surfaces. The insulated surfaces are the ones positioned near the electrodes, which are used to avoid the presence of the breakdown phenomena. The other surfaces are considered grounded therefore, a null electric potential is imposed on them. An overview of the used boundary conditions and numerical schemes is reported in Tab. 1. Regarding the turbulence model, the k-epsilon model [19] is selected for the specific application since it supplies, according to the literature, good performances in the case of low-reynolds shear flows.

The mesh is constructed with the CFMesh suites of the OpenFOAM-v2206 software, which allows the creation of un-

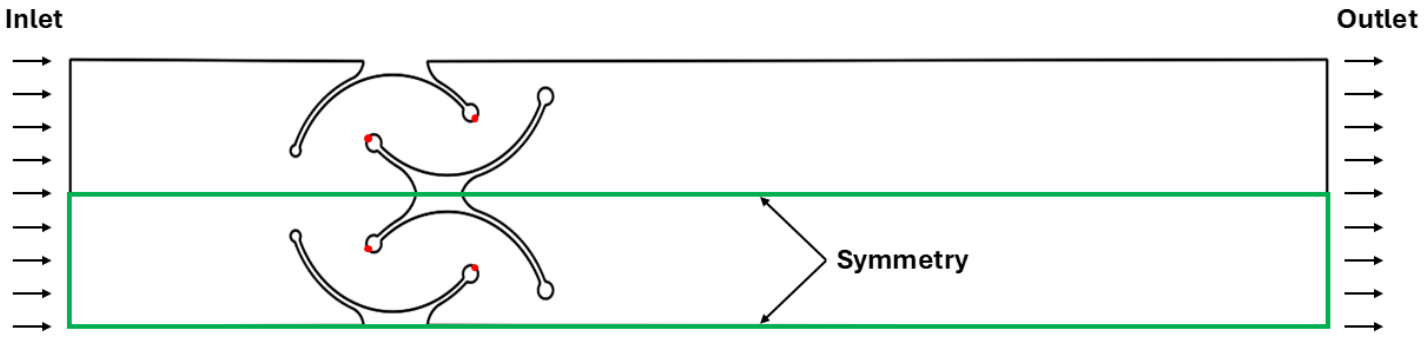

FIGURE 1: Sketch of the used numerical domain

TABLE 1: Boundary conditions and numerical scheme

Inlet	Fixed velocity
Outlet	Impose static pressure
Upper/lower surface	Symmetry
Insulated surfaces	No-slip wall
Grounded surfaces/ electrodes	No-slip wall with imposed V
Electrodes $\rho_c - \mathbf{E}$	Peek
Advective	Linear upwind
Time	Steady state
Turbulence	Linear Upwind

structured hexahedral mesh. A grid sensitivity analysis is performed by observing the mean pressure at the inlet of the domain and the force acting on the filter elements. The convergence is reached with a number of elements approximately equal to 40e3. Initially, only the continuous phase is solved, and the solid particles are introduced into the fluid domain only once the convergence of the flow fields is reached. The properties and size of the used solid particles are reported in Tab. 2. The diameter distribution is selected according to [8] to represent the solid particles typically found at the inlet of a gas turbine located in the proximity of a polluted urban environment. The number of particles per second injected at the inlet of the domain, instead, is selected to test the device in an extreme environmental condition, e.g. sandstorm.

TABLE 2: Details of the used particulate

	Value
Particle density $[kg/m^3]$	2700
Particle per second	403.19×10^3
Type of Distribution	Normal
Mean diameter $[\mu m]$	1.0
Variance $[\mu m]$	0.5
Max Diameter $[\mu m]$	3.0
Min Diameter $[\mu m]$	0.5

Different approaches can be employed to model the interaction between the fluid medium and the particles. To reduce the computational effort of the simulations, a one-way coupling is used to model the particle behaviors inside the filter, with the assumption that the solid particles exert no influence on the continuous phase. The effect of the turbulence on the particles' behavior is taken into account using a stochastic approach which samples a Gaussian plus delta distribution to calculate the velocity fluctuation. In addition, within the lagrangian equilibrium, the electrostatic and spherical drag forces are introduced. Furthermore, upon impact with the boundary, the particles are subject to elastic and dissipative forces. The magnitude of the dissipative force is a function of the restitution coefficient assigned to the specified boundary. In particular, a restitution factor equal to one, i.e., complete elastic rebound, is prescribed for all the surfaces except the grounded one, where a restitution factor equal to zero is set. Therefore, the particles are trapped. This assumption is generally incorrect since the Coulomb force acting on the particle could not completely overcome the impact force. Based on the experimental evidence of the authors on the considered setup [12], the total number of particles that impact a grounded surface and leave it is very low compared to that impacting an isolated surface. In light of this observation and the difficulty of estimating normal and tangential restitution factors, the assumption of adherence to ground surfaces is considered plausible.

2.2 Geometry parametrizations and optimization algorithm

Filter elements are composed of mirrored curved surfaces that are arranged in a systematic array, thereby adopting a modular approach. This choice constitutes an extreme constraint on the geometrical optimization. Moreover, another constraint is related to the avoidance of the electric breakdown. To ascertain the inception of a spark within the fluid domain, the authors have employed the following criterion: a breakdown occurs if the electrical field along a connecting path between the electrode and the grounded surfaces reaches a value exceeding 3 MV/m (which represents the dielectric strength of pure air). This constraint could be translated into a prescribed minimum distance between the grounded surfaces. The considered filtration system aims to provide an alternative to the medium-high filtration mechanical filters currently employed in gas turbine applications. Therefore, the pressure drops associated with the innovative filter should not exceed the values typically observed with traditional filtering media. A threshold value for the pressure drop is considered inside the optimization process to ensure that the system operates within the desired pressure drop range. This limit is fixed at 100 Pa, which corresponds to the order of magnitude of that observed for a high-efficiency mechanical filter. In addition, the selected threshold allows the use of multiple elements in the direction of airflow to further increase the capture efficiency of the unit. As the first attempt, the baseline geometry is approximated and parametrized as a single arc, and the body of the filter elements is considered a vertical line. Considering the usage of specular filtering elements and maintaining the same root width for structural reasons, the geometry is completely described once the position of the arc's vertices is known. Therefore, the single arc parametrization is characterized by four degrees of freedom, corresponding to the position of the extreme arc points in the plane. The second proposed parametrization instead involves two arcs joined at the end of the root of the element. In this case, the geometry is wholly described once the positions of the extreme points and the arc centers are known. Four additional degrees of freedom, the coordinates of the centers, are added to the system compared to the first approach. Figure 2 shows a sketch of the implemented parametrization, where the points moved by the optimizer are highlighted with a cross (orange extreme points, violet arcs' centers).

The optimization tool is written using Python programming language and includes geometry construction, setup of the simulation, execution of the simulation, post-processing of the results, and geometry optimization. The different phases of a CFD simulation and the post-processing are automatically managed by the tool. The geometry is generated using SALOME, an open-source CAD and meshing software. In particular, the abovementioned geometrical parameterizations are coded inside the Python code

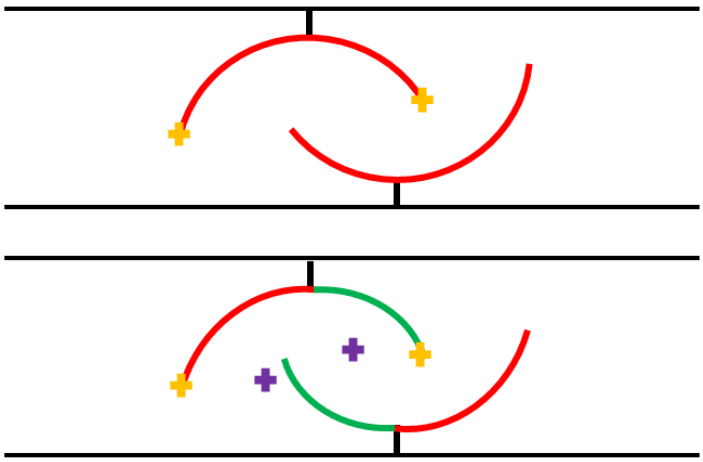

FIGURE 2: Filter element parametrizations: single arc (top) and double arc (bottom)

that uses the SALOME API to design the filter according to the input parameters, which are degrees of freedom for the considered geometry. Regarding the post-processing, the code analyzed the results files of the simulation. In particular, the capture efficiency and the area average of the inlet static pressure, therefore, the pressure drop of the system are calculated. The Simplicial Homology Global Optimizer, SHGO, included in the Python Scipy [20] library, is selected to maximize the system's capture efficiency. The selected optimization algorithm required as input the variables' range of variability, and the number of iterations to construct the simplicial complex. Once the parameterization is fixed, the number of variables, therefore the number of degrees of freedom, is fixed. At the same time, the range of variability of the parameters is selected to avoid overlap between the upper and lower elements. The SHGO algorithm has been developed to minimize a function of one or more variables; therefore, since the object is to maximize the capture efficiency, its inverse is used as the objective function.

3. RESULTS

In the first part of the chapter, the baseline geometry and its performance are described. Moreover, the effects of both applied electric potential and extension of the collecting area on the capture efficiency are discussed. Subsequently, the validation of the optimizer in the inertial-only configuration is reported. Finally, the results for both single-arc and double-arc parametrization are shown for the multiphysics, inertial-electrostatic combined configuration.

3.1 Baseline geometry description

The baseline geometry of the element was developed in [11], through a trial-and-error process that was finalized to maximize the capture efficiency and minimize the pressure drop. A very high efficiency, approximately equal to 99 %, was obtained with the two wires configuration when an electric potential equal to 45 kV was applied to them. Figure 3 shows the geometry of the baseline filter elements, where red dots highlight the position of the electrodes and green curves indicate the position of the grounded surfaces. From the previous sensitivity analysis, the capture efficiency of the system strongly depends on the applied electric potential. In particular, in the case of a single wire configuration, in which only the upper element presents the wire, a linear decrease of the capture efficiency as a function of the applied potential was established [11]. The other important parameter that influences the capture efficiency of the system is the dimension of the collecting area, i.e. grounded surfaces. For this reason, a sensitivity analysis on the extension of the grounded area extension is performed. The results of these analyses indicated that an increase in the collecting area enhanced the system's efficiency. However, this outcome is once again constrained by the breakdown condition.

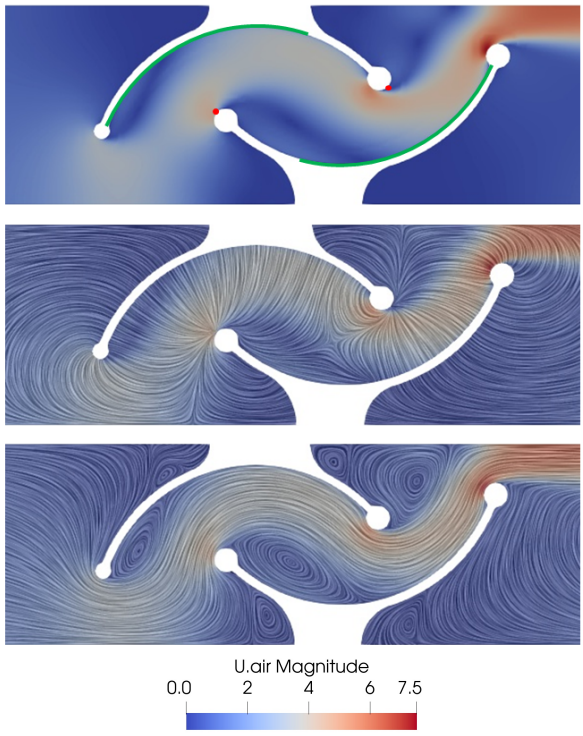

FIGURE 3: Baseline filter geometry: velocity contour (top), the electrical field's convolution line (mid) and streamline plot (bottom)

The aim of the work is to extend the applicability of this filtration system in case of a lower voltage power supply. For this reason, a geometrical optimization is necessary to recover the performance loss due to the reduced applied potential. The electric potential considered for this application is equal to 12 kV, therefore more than three times lower than in the original setup. The performance of the baseline geometry and the electrical configuration utilized, e.g. applied electrical potential, number, and size of the wires, is reported in Tab. 3. The approximately zero efficiency of inertial-only and the extremely low pressure drops indicate that an effective approach to increasing the combined electrostatic-inertial efficiency might be to improve the inertial contribution, despite the potential increase in pressure drops.

TABLE 3: Baseline geometry performance and characteristics

	Value
Number of wires	2
Wire radius [mm]	0.154
Electric potential [kV]	12.0
Combined capture efficiency [%]	18.2
Inertial only capture efficiency [%]	0.0
Pressure drop [Pa]	50.0

3.2 Validation of the optimizer

To validate the optimizer results, two optimizations are performed using the single-arc parameterization, keeping the extension of the collecting area constant while the system operates in inertial-only mode. The first optimization is conducted to maximize the capture efficiency of the system, while the second is performed to reduce pressure losses. The original configuration, which can be approximated to a single arc geometry, is considered the starting point of the optimization. The two elements are expected to become closer in the efficiency optimization, resulting in an increased pressure drop. Conversely, the elements are expected to become more open and located far from each other in pressure drop optimization.

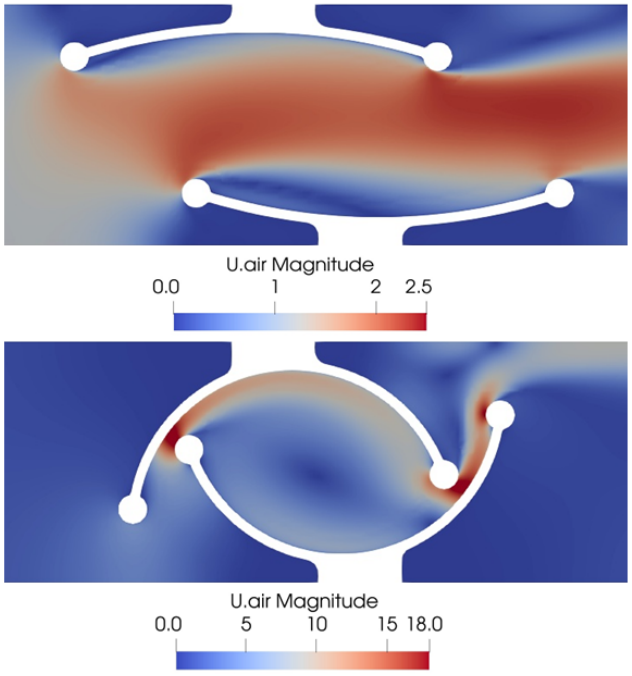

FIGURE 4: Velocity magnitude contours for the inertial-only optimized configurations: minimal pressure drop (top) and maximum capture efficiency (bottom)

Figure 4 shows the results of both the efficiency and pressure drop optimizations in the inertial-only configuration. As expected, the optimizer closed and opened the elements. The pressure drop optimization shows a reduction of approximately 42 Pa compared to the original case. In the pressure drop optimization, an increase in both capture efficiency and pressure drop is observed. In particular, an inertial-only efficiency of 3.8% and a pressure drop of 350 Pa are obtained. Therefore, the optimization tool can be considered validated for pressure loss and capture efficiency optimizations.

3.3 Combined inertial-electrostatic optimization

The results of the multiphysics inertial-electrostatic optimization, performed with the single and double arc parameterizations, are reported below. During the optimization, the capture area is kept at a maximum consistent with the minimum distance between the electrode and the ground surface to avoid breakdown and maximize efficiency. In addition, the number and dimensions of the wires are kept the same as in the baseline case.

In the single arc parameterization, the optimizer can move only the extreme points of the arc. Instead, the center point is fixed in the same position as the single arc approximation of the base geometry. The upper half element is taken as a reference for the geometrical comparison. The optimized elements are characterized by a higher radius than the original configuration. Moreover, the arc's extreme points are shifted toward the outlet and upward than in the baseline geometry. Figure 5 shows the optimal geometry obtained with the single arc configuration, where red dots highlight the position of the wires and green arcs show the grounded surfaces.

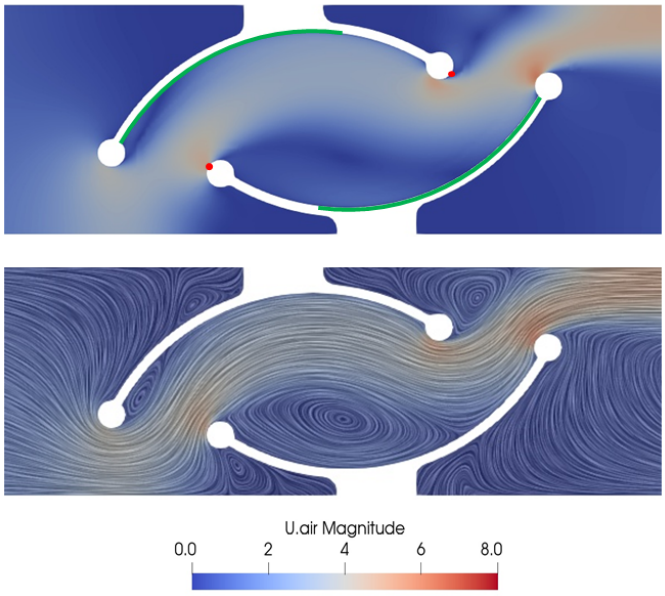

FIGURE 5: Single arc configuration inertial-electrostatic optimization: velocity contour (top) and, streamlines plot (bottom)

At first glance, the geometry looks similar to the original despite these geometric changes. However, a significant difference in capture efficiency and pressure losses is detected. In particular, the capture efficiency results equal to 21.5 %, which is 18.1% higher than the baseline one. The increase in efficiency is achieved in two steps. In the first step, the lower element creates a large separation zone within the channel, causing particles carried by the airflow to flow more toward the upper element than in the original configuration. In addition, the flow is directed

toward the lower element in the terminal part of the device. In the second step, the electrostatic force pushes the particles into the grounded surfaces, i.e., the concave/convex surfaces of the lower/upper elements, and thanks to the continuous application of the electric field, the particles are collected. Another advantage of the optimized geometry is related to reducing the system's pressure losses. Specifically, the optimized configuration is characterized by pressure losses of about 30 Pa, which represent a 40% reduction in comparison to the baseline configuration (50 Pa).

In the double arc parameterization, the optimizer can move both extreme points and centers of the arcs. The common extreme vertex of the arcs is another time fixed in the same position as the baseline geometry one. The result of this optimization is shown in Fig. 6. In this case, the element geometry is significantly different than both baseline and single arc optimized ones. The extreme points of the arcs are moved by the optimizer toward the inside of the device and the lower element. The con of this closure is the increase in the pressure drops of the device. Specifically, the pressure drops of the filter are equal to 71 Pa, which are 42 % and 136 % higher than the baseline and the single arc optimized configurations. Nevertheless, the pressure drops are significantly lower than the one of a conventional high-efficiency porous filter, approximately equal to 500 Pa.

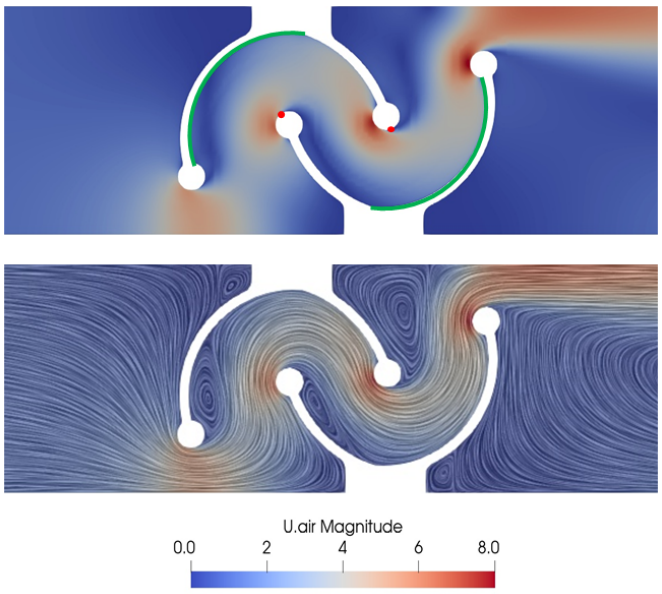

FIGURE 6: Double arc configuration inertial-electrostatic optimization: velocity contour (top) and, streamlines plot (bottom)

The advantage of the optimized two arcs configuration is the significant increase in the capture efficiency of the system, which is equal to 25.1 %. Compared to the other geometries, a capture efficiency enhancement respectively equal to 37.9 %, baseline, and 16.7 %, single arc, are obtained. The improvement in efficiency is not limited to the approach outlined above for the single-arc configuration. In addition to the presence of separation zones that direct the flow toward the grounded surfaces, the mean velocity inside the device is increased due to the device's more closed configuration. As the flow velocity increases, the efficacy of inertial separation also rises. This indicates that the improvement in combined efficiency is associated with the increasing importance of this separation mechanism. The overall performance of the baseline geometry and the optimized ones are reported in Tab. 4.

TABLE 4: Baseline geometry performance and characteristics

	Pressure drop [Pa]	η_c [%]
Baseline configuration	50	18.2
Single arc optimized	30	21.5
Double arc optimized	71	25.1

4. CONCLUSIONS

The work shows a geometrical multi-physics optimization of an innovative electro-dynamic filter for gas turbine applications. The initial part of the study introduces the optimizer, emphasizing the incorporated geometrical parametrization and the utilized optimization algorithm. Subsequently, the optimization is validated in the inertial-only modality, given that the impact of the electrostatic field was demonstrated in previous research. In particular, two objective functions are used to validate the tool. In the first optimization, the objective is to reduce pressure losses, while in the secondary optimization, the aim is to enhance the capture efficiency of the system. The optimizer has opened and closed the filter branches respectively to decrease the pressure losses and increase the capture efficiency. Accordingly, the optimization tool may be considered validated. In the final phase of the study, a multiphysics optimization is conducted using both single and double-arc geometrical parametrization to enhance the capture efficiency while maintaining pressure drops below a specified threshold value. The threshold value is set equal to 100 Pa, approximately the order of magnitude of the pressure drop that characterizes a traditional porous filter. The optimized geometries showed a significant improvement in capture efficiency compared to the base element, with values 18.1 % and 37.9 % higher for single and double arc configurations respectively. However, the single arc configuration also exhibits a lower pressure drop than the baseline configuration, with a value of 30 Pa compared to 50 Pa. The double arc configuration, instead, is distinguished by a slightly elevated pressure loss of 71 Pa. Nevertheless, the resulting values remain markedly inferior to those associated with the porous filter system typically employed in a gas turbine, i.e., 500 Pa. Further investigations will be carried out to evaluate the effects of other types of geometric parameterization and the use of an array of filter elements on the capture efficiency of the system. An experimental program will also be carried out to validate the results of the CFD-based geometric optimization.

REFERENCES

[1] Tarabrin, AP, Schurovsky, VA, Bodrov, AI and Stalder, J-P. "An analysis of axial compressor fouling and a blade cleaning method." (1998).

[2] Chen, Shaowen, Zhang, Chen, Shi, Hui, Wang, Songtao and Wang, Zhongqi. "Study on the impact of fouling on

axial compressor stage." *Turbo Expo: Power for Land, Sea, and Air*, Vol. 44748: pp. 1–8. 2012. American Society of Mechanical Engineers.

[3] Igie, Uyioghosa, Pilidis, Pericles, Fouflias, Dimitrios, Ramsden, Kenneth and Laskaridis, Panagiotis. "Industrial gas turbine performance: compressor fouling and on-line washing." *Journal of turbomachinery* Vol. 136 No. 10 (2014): p. 101001.

[4] Casari, Nicola, Pinelli, Michele, Spina, Pier Ruggero, Suman, Alessio and Vulpio, Alessandro. "Performance degradation due to fouling and recovery after washing in a multistage test compressor." *Journal of Engineering for Gas Turbines and Power* Vol. 143 No. 3 (2021): p. 031020.

[5] Suman, Alessio, Morini, Mirko, Aldi, Nicola, Casari, Nicola, Pinelli, Michele and Spina, Pier Ruggero. "A compressor fouling review based on an historical survey of asme turbo expo papers." *Journal of Turbomachinery* Vol. 139 No. 4 (2017): p. 041005.

[6] Suman, Alessio, Casari, Nicola, Fabbri, Elettra, di Mare, Luca, Montomoli, Francesco and Pinelli, Michele. "Generalization of particle impact behavior in gas turbine via non-dimensional grouping." *Progress in Energy and Combustion Science* Vol. 74 (2019): pp. 103–151.

[7] Casari, Nicola, Pinelli, Michele, Suman, Alessio, di Mare, Luca and Montomoli, Francesco. "EBFOG: deposition, erosion, and detachment on high-pressure turbine vanes." *Journal of Turbomachinery* Vol. 140 No. 6 (2018): p. 061001.

[8] Wilcox, Melissa, Baldwin, Richard, Garcia-Hernandez, Augusto and Brun, Klaus. "Guideline for gas turbine inlet air filtration systems." *Gas Machinery Research Council, Dallas, TX* (2010).

[9] "High efficiency air filters (EPA, HEPA and ULPA) - Part 1: Classification, performance testing, marking." Standard. European committee for Standardization, Bruxelles,BRU. 2009.

[10] He, Zhongjie, Dass, ET Mohan and Karthik, Girish. "Design of electrostatic precipitator to remove suspended micro particulate matter from gas turbine inlet airflow: Part I. Experimental study." *Journal of Aerosol Science* Vol. 108 (2017): pp. 14–28.

[11] Pinelli, Michele, Piovan, Mattia, Suman, Alessio, Zanini, Nicola, Rossin, Stefano and Minotti, Stefano. "Numerical implementation of electrostatic solver within OpenFOAM for GT intake filtration." *Turbo Expo: Power for Land, Sea, and Air*, Vol. 88063: p. V12BT31A010. 2024. American Society of Mechanical Engineers.

[12] Zanini, Nicola, Suman, Alessio, Piovan, Mattia, Pinelli, Michele, Rossin, Stefano and Minotti, Stefano. "An Innovative Filtering Apparatus for Gas Turbines." *Turbo Expo: Power for Land, Sea, and Air*, Vol. 88018: p. V009T19A019. 2024. American Society of Mechanical Engineers.

[13] Penney, Gaylord W and Matick, Richard E. "Potentials in DC corona fields." *Transactions of the American Institute of Electrical Engineers, Part I: Communication and Electronics* Vol. 79 No. 2 (1960): pp. 91–99.

[14] Parasram, N. "Particle motion in electric precipitators." (2001).

[15] Nikas, KSP, Varonos, AA and Bergeles, GC. "Numerical simulation of the flow and the collection mechanisms inside a laboratory scale electrostatic precipitator." *Journal of electrostatics* Vol. 63 No. 5 (2005): pp. 423–443.

[16] Choi, Ho Yeon, Park, Yong Gap and Ha, Man Yeong. "Numerical study on the effect of staggered wire electrodes in an electrostatic precipitator." *Journal of Mechanical Science and Technology* Vol. 34 (2020): pp. 3303–3310.

[17] Farnoosh, Niloofar, Adamiak, K and Castle, GSP. "3-D numerical analysis of EHD turbulent flow and mono-disperse charged particle transport and collection in a wire-plate ESP." *Journal of Electrostatics* Vol. 68 No. 6 (2010): pp. 513–522.

[18] Lawless, Phil A. "Particle charging bounds, symmetry relations, and an analytic charging rate model for the continuum regime." *Journal of Aerosol Science* Vol. 27 No. 2 (1996): pp. 191–215.

[19] Launder, Brian Edward and Spalding, Dudley Brian. "The numerical computation of turbulent flows." *Numerical prediction of flow, heat transfer, turbulence and combustion*. Elsevier (1983): pp. 96–116.

[20] Virtanen, Pauli, Gommers, Ralf, Oliphant, Travis E., Haberland, Matt, Reddy, Tyler, Cournapeau, David, Burovski, Evgeni, Peterson, Pearu, Weckesser, Warren, Bright, Jonathan, van der Walt, Stéfan J., Brett, Matthew, Wilson, Joshua, Millman, K. Jarrod, Mayorov, Nikolay, Nelson, Andrew R. J., Jones, Eric, Kern, Robert, Larson, Eric, Carey, C J, Polat, İlhan, Feng, Yu, Moore, Eric W., VanderPlas, Jake, Laxalde, Denis, Perktold, Josef, Cimrman, Robert, Henriksen, Ian, Quintero, E. A., Harris, Charles R., Archibald, Anne M., Ribeiro, Antônio H., Pedregosa, Fabian, van Mulbregt, Paul and SciPy 1.0 Contributors. "SciPy 1.0: Fundamental Algorithms for Scientific Computing in Python." *Nature Methods* Vol. 17 (2020): pp. 261–272. DOI 10.1038/s41592-019-0686-2.